COOPER, M. & NATHANS, R. (1967). *Acta Cryst.* **23**, 357-367.
COWLEY, R. (1987). *Acta Cryst.* **A43**, 825-836.
FEIDENHANS'L, R. (1989). *Surf. Sci. Rep.* **10**, 105-188.
FEIDENHANS'L, R., PEDERSEN, J., NIELSEN, M., GREY, F. & JOHNSON, R. (1986). *Surf. Sci.* **178**, 927-933.
GIBBS, D., OCKO, B., ZEHNER, D. M. & MOCHRIE, S. (1988). *Phys. Rev. B*, **38**, 7303-7310.
KASHIHARA, Y., KIMURA, S. & HARADA, J. (1989). *Surf. Sci.* **214**, 477-492.
LUCAS, C., GARTSTEIN, E. & COWLEY, R. (1989). *Acta Cryst.* **A45**, 416-422.
LUCAS, C., HATTON, P., BATES, S., RYAN, T., MILES, S. & TANNER, B. (1988). *J. Appl. Phys.* **63**, 1936-1941.
MARRA, W., EISENBERGER, P. & CHO, A. (1979). *J. Appl. Phys.* **50**, 6927-6933.
OCKO, B., GIBBS, D., HUANG, K., ZEHNER, D. & MOCHRIE, S. (1991). *Phys. Rev. B*, **44**, 6429-6443.
PYNN, R., FUJII, Y. & SHIRANE, G. (1983). *Acta Cryst.* **A39**, 38-46.
RABEDEAU, T., TONEY, M., HARP, G., FARROW, R. & MARKS, R. (1992). Unpublished.
ROBINSON, I. (1986). *Phys. Rev. B*, **33**, 3830-3836.
ROBINSON, I. (1988). *Aust. J. Phys.* **41**, 359-367.
ROBINSON, I. (1989). *Rev. Sci. Instrum.* **60**, 1541-1544.

ROBINSON, I. (1991). In *Handbook on Synchrotron Radiation*, Vol. 3, edited by G. S. BROWN & D. E. MONCTON, pp. 221-266. Amsterdam: North Holland.
SAMANT, M., BROWN, C. & GORDON, J. (1991). *Langmuir*, **7**, 437-439.
SAMANT, M., TONEY, M., BORGES, G., BLUM, L. & MELROY, O. (1988a). *Surf. Sci.* **193**, L29-L36.
SAMANT, M., TONEY, M., BORGES, G., BLUM, L. & MELROY, O. (1988b). *J. Phys. Chem.* **92**, 220-225.
SANDY, A., MOCHRIE, S., ZEHNER, D., HUANG, K. & GIBBS, D. (1991). *Phys. Rev. B*, **43**, 4667-4687.
TONEY, M., FARROW, R., MARKS, R., HARP, G. & RABEDEAU, T. (1992). *Proc. Mater. Res. Soc.* **263-F2**, 273-280.
TONEY, M., GORDON, J., KAU, L., BORGES, G., MELROY, O., SAMANT, M., WIESLER, D., YEE, D. & SORENSEN, L. (1990). *Phys. Rev. B*, **42**, 5594-5603.
TONEY, M., GORDON, J., SAMANT, M., BORGES, G., MELROY, O., YEE, D. & SORENSEN, L. (1992). *Phys. Rev. B*, **45**, 9362-9374.
TONEY, M. & MELROY, O. (1991). In *Electrochemical Interfaces: Modern Techniques for In-Situ Interface Characterization*, edited by H. D. ABRUNA, pp. 57-129. Berlin: VCH Verlag Chemie.
WARREN, B. (1969). *X-ray Diffraction*. Reading, MA: Addison-Wesley.

The Correction of Geometrical Factors in the Analysis of X-ray Reflectivity

BY A. GIBAUD AND G. VIGNAUD

Laboratoire PEC UA no. 807 CNRS, Université du Maine, 72017 Le Mans CEDEX, France

AND S. K. SINHA

Exxon Research Laboratory, Annandale, NJ 08801, USA

Abstract

X-ray reflectivity is a powerful technique to study electron density profiles in the direction normal to the surface of a flat sample. As usual in scattering experiments, where the phase information is lost, it is necessary to build a model that can be used to calculate the reflectivity for comparison with the measured reflectivity. In the calculations, it is necessary to correct the calculated reflectivity from geometrical and resolution-function factors, which play a major role at low angles of incidence. These factors are presented in this paper and the corrected calculated intensity is compared with the measured reflectivity of a commercial silicon wafer and of a niobium film on a sapphire substrate.

1. Introduction

X-ray reflectivity is now widely used to determine the structure and the composition of flat surfaces in the direction normal to the sample face. The object of the reflectivity measurement is to determine the depth profile of electron density inside the material. The technique is highly appropriate to investigations of multilayers and polymer, magnetic and ferroelectric thin layers and also liquid surfaces (Russel, 1990; Als-Nielsen, 1984; Benatar, 1992). Such systems are of considerable scientific and industrial interest because their properties may differ considerably from those of the bulk materials, as is the case in magnetic ultrathin layers, and because periodic variation of the composition (as in multilayers) causes further differences in properties. In addition, the cost of thin layers is low compared with that of the bulk materials. Furthermore, thin layers are useful for insertion into integrated electronics, as, for example, with ferroelectric nonvolatile memories.

The measurement of X-ray reflectivity is in principle easy to carry out, especially for samples with large flat surfaces. However, even in this case, the finite size of the surface, combined with the non-

negligible absorption of the X-ray beam and the uncertainty in the size of the beam spot at the sample location, introduce some difficulties, although they can be overcome in practice. The aim of this paper is to describe a methodology for the measurement of X-ray reflectivity based upon the experimental determination of geometrical factors that are relevant in the measurement and in the data reduction of X-ray specular reflectivity. We shall assume that the sample is ideally terminated and that diffuse scattering is negligible compared with the true specular reflectivity (Sinha, 1991).

II. Experimental set-up

II.1. Description of the diffractometer

The measurement of X-ray reflectivity from a flat surface may be made with a diffractometer whose detector arm (at an angle 2θ to the direct beam) may be moved independently of the sample (at an angle α to the direct beam). The sample must be mounted on an $X-Y$ translation table so that the sample may be brought into the beam and its position finely adjusted. It is also advisable to mount it on a goniometer head to bring the normal to the face into the scattering plane. A set of adjustable slits is necessary to cut the beam to the correct size (front slits) and to collimate the scattered beam (back slits). With a normal tube, a pyrolitic graphite monochromator may be used, located behind the back slits, to select the $K\alpha$ lines of the target. With such a set-up and with a Cu tube operating at 40 kV and 30 mA, a flux of 10^7 photons mm^{-2} s^{-1} is available in the direct beam. This flux is certainly very small compared with the flux available from a synchrotron (10^{10} photons mm^{-2} s^{-1}) or a rotating anode (10^9 photons mm^{-2} s^{-1} with a graphite monochromator). Nevertheless, as the range of reflectivity usually measurable with X-rays is from 1 to 10^{-8} (at the very best), measurements of reflectivity are possible with a normal tube provided that the background does not exceed 1 count s^{-1}. The limiting value of measurable specular reflectivity is indeed the background level under the true specular signal, which is due to diffuse scattering by static or dynamical processes or to air diffusion. A background of 1 count s^{-1} or less can be achieved with an appropriate collimation.

Let us note that, with such a range of reflectivities, it is necessary to attenuate the direct beam at low angles of incidence. Indeed, most of the detectors have an upper limit of saturation that is of the order of 4×10^4 count s^{-1}.

II.2. The choice of front slits

The aperture of the front slits is determined by the size L of the sample. It is straightforward to show

that if the direct beam is perfectly collimated and uniform (an assumption that is not generally true, as we shall see later), makes an incident angle α with the surface of the sample (see Fig 1) and has a thickness T (which depends on the aperture of the front slits) then the footprint of the beam on the sample is

$$F = T/\sin \alpha. \tag{1}$$

A correct choice for the front slits is one for which

$$D = T/\sin \alpha < L \quad \text{for } \alpha \simeq \alpha_c, \tag{2}$$

where α_c is the critical angle for total reflection. Let us bear in mind that α_c is always very small (of the order of 0.3°), hence (2) is not always fulfilled. As an example, if we fix $\alpha_c = 0.2°$ and $L = 35$ mm, we must have $T < 0.12$ mm.

This example gives an idea about the size of the front slits that must be used to achieve total reflection of the X-ray beam below the critical angle. Clearly, this condition becomes more severe for smaller critical angles and reduction of the size of the front slits becomes difficult, though not impossible. In addition, the uncertainty in the real size of such small apertures or in the real thickness of the beam at the sample location creates some difficulties, which can, however, be experimentally overcome, as we shall see later.

II.3. The choice of back slits

The aperture of the back slits has to match that of the front slits. This reduces the background and achieves a good resolution without too much loss of intensity. If the front and back slits are matched correctly, then a 2θ scan of the direct beam, considered as uniformly distributed, has a shape given by

$$I(2\theta) = I_0 \Pi_\alpha(2\theta) * \Pi_\alpha(2\theta), \tag{3}$$

where I_0 is the direct-beam intensity, $\Pi_\alpha(2\theta)$ is a step function of angular aperture α [full width at half-maximum (FWHM)] and the symbol $*$ denotes the convolution operation. The convolution of two step
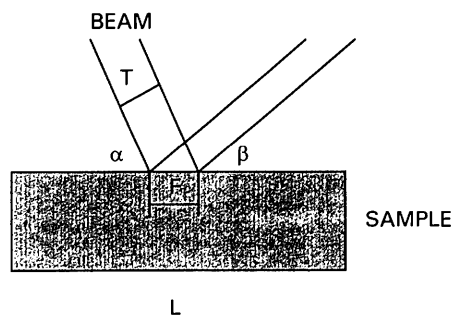

Fig. 1. Diagram of the footprint of the beam for an incident angle α of the direct beam on the surface of the sample.

functions of the same aperture is a triangular function; thus, for matching front and back slits, the direct beam is triangularly shaped, as shown in Fig. 2(a). Equation (3) is only valid if the monochromator mosaic spread is large compared with the angular acceptance of the slits; otherwise, it is necessary to convolve the step functions with the mosaic-spread distribution function of the monochromator. In addition, the direct beam is often not uniformly distributed and is then better described by a Gaussian function $g(2\theta)$ than a step function. As a result, a 2θ scan of the detector through the direct beam usually deviates from a triangular function and has tails that decrease relatively smoothly to zero (see Fig. 2b). The intensity is then given by

$$I(2\theta) = G(2\theta) * \Pi_\alpha(2\theta). \qquad (4)$$

II.4. The sample alignment

The sample is first aligned in the direct beam by setting the detector angle to $2\theta = 0$ and translating the sample holder so as to halve the intensity of the
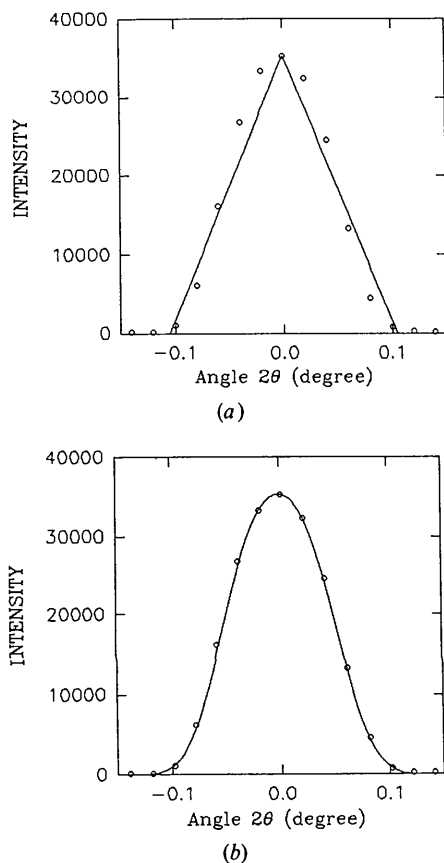

(a)

(b)

Fig. 2. Result of the convolution of (a) two step functions and (b) a step function with a Gaussian function, together with the direct beam (open circles). In (b) the solid line corresponds to the best fit, leading to $T_d = 120$ and $T_r = 105$ μm.

direct beam. Then the parallelism of the sample face with the direct beam is ensured by rotating the sample about its axis. During this procedure, the edges of the sample cut the remaining half-strength of the direct beam and the intensity collected by the detector should steadily decrease with the sample rotation. If the intensity increases during the rotation of the sample, the sample face is too far from the beam and it must be moved closer until the intensity always decreases from a value of half the total beam intensity.

Once this procedure has been carefully followed, the sample is in principle correctly set and the reflectivity measurement can begin. It is also worth checking the alignment at a position close to the critical angle. At this point, the reflectivity curve is a ridge, which follows Fresnel's law in Q parallel to the normal of the face (denoted Q_z in the following) and is extremely narrow in the perpendicular direction (denoted Q_x in the following). Any mis-setting of the sample is then easily discovered and corrected.

II.5. Different ways to measure the reflectivity

The reflectivity measurements can be carried out in accordance with various procedures. The choice of procedure depends upon the way the surface is terminated. If the surface is ideally terminated, i.e. does not present any correlated fluctuations of electron density, then it is possible to measure the reflectivity directly using a longitudinal or a θ–2θ scan along the specular ridge. This is the simplest and the quickest way to measure the reflectivity but it is very important to check that the scan is always along the top of the specular ridge, which is very narrow. The absolute reflectivity $R(2\theta)$ is given, for the case where all the beam is intercepted, by

$$R(2\theta) = I(2\theta)/I_0, \qquad (5)$$

where I_0 is the direct-beam intensity and $I(2\theta)$ is the intensity at the angular position 2θ of the detector after background subtraction.

When the sample is not ideally terminated, i.e. presents some diffuse scattering in the transverse scans across the ridge, it is then necessary to perform transverse scans to obtain the true specular reflectivity, which is the intensity substracted from the diffuse scattering. In this case, it is possible to perform two kinds of scans: transverse q_x scans or angular α scans.

For the angular scan, the absolute reflectivity is given by

$$R(2\theta) = \int I(\alpha, 2\theta) \, d\alpha / [\tfrac{1}{2} \int I_0(2\theta_0) \, d(2\theta_0)], \qquad (6)$$

where $I_0(2\theta_0)$ is the intensity of the direct beam, in the absence of the sample, at the position 2θ of the detector and $I(\alpha, 2\theta)$ is the intensity across the ridge at the position α of the sample and 2θ of the detector.

For the q_x scan, the steps are given by $dq_x = Q_z\, d\alpha$ and the absolute reflectivity is given by

$$R(2\theta) = Q_z^{-1} \int I(q_x, 2\theta)\, dq_x / [\tfrac{1}{2}\int I_0(2\theta_0)\, d(2\theta_0)].$$
(7)

III. Determination of the geometrical factors

III.1. Determination of the real thickness of the beam

The sample-alignment procedure can be used to find the exact thickness of the beam at the sample location. This thickness T, which we shall consider as the FWHM of the nonuniform beam, is a key parameter for the correction of the real intensity reflected by the sample when the condition given in (2) is not fulfilled. With the assumption that the sample is correctly set in the main beam, described by a Gaussian $g(t)$ (t being the beam thickness), the intensity collected by the detector set at $2\theta = 0$ at a position α of the sample is given by

$$I(\alpha) = (I_0/2)\left(1 - \int_0^{t_s} g(t)\, dt \middle/ \int_0^{t_d/2} g(t)\, dt\right),$$
(8)

where $g(t)$ is given by

$$g(t) = A \exp(-t^2/2\sigma^2),$$
(9)

σ being the half-width at half-maximum (HWHM) of the main beam, which verifies $T = 2\sigma$; t_d is the linear width of the detector and t_s is given by

$$t_s = L|\sin \alpha|/2.$$
(10)

Equation (8), which is valid if the sample is rotated about its axis of symmetry, gives the intensity measured at a fixed position of the detector as a function of the angle α. Any asymmetry in the shape is a sign that the sample is incorrectly set (i.e. is not symmetric about the axis of rotation). The above function can be fitted to the data with the real thickness $T_r = 2\sigma$ of the beam at the sample location and with the detector width T_d as parameters, as shown in Fig. 2. In our case, we find that the real thickness of the beam, T_r, is in good agreement with the thickness T of the slits (which are adjustable Huber slits). Thus if the slits are located close to the sample then the spread of the direct beam is negligible.

The knowledge of $\sigma = T_r/2$ allows the geometrical corrections of the reflected intensity when the nonuniform footprint of the beam is larger than the sample width. The corrected reflected intensity at the position 2θ of the detector is given by

$$I_c(2\theta) = I(2\theta) \int_0^{L(\sin \alpha)/2} g(t)\, dt \middle/ \int_0^{t_m} g(t)\, dt,$$
(11)

where $I(2\theta)$ is the calculated intensity according, for example, to the matrix method and t_m is the value at which the intensity of the direct beam is considered to be zero.

If the beam is uniform and given by a step function of FWHM equal to T_r, then the corrected intensity is reduced to the following simple expression, which is linear in α,

$$I_c(2\theta) = I(2\theta)\, L(\sin \alpha)/T_r$$

$$= I(2\theta)\, L\alpha/T_r.$$
(12)

Fig. 3 shows the results of such calculations: there is a marked difference in the behavior of the reflected intensity for a Gaussian beam (nonlinear reflectivity) and a step-function beam (linear reflectivity). In both cases, the reflected intensity becomes zero when α is zero, since the footprint of the beam is then infinite. Nevertheless, the correction to apply close to $\alpha = 0$ is a bit more complicated than that proposed in (11) and (12). Indeed, although at $\alpha = 0$ the sample does not reflect any intensity, it lets half of the direct beam fall into the detector. During a θ–2θ scan, the measured intensity is then the sum of the decreasing intensity coming from the direct beam and of the increasing intensity reflected by the sample, as shown for a typical case in Fig. 4 and observed by Brugemann, Bloch, Press & Gerlach (1990). In addition, a further complication is that the direct beam is no longer at the position $2\theta = 0$ in the presence of the sample, although it was perfectly centered in its absence. This is because the presence of the sample modifies the direct-beam repartition of intensity viewed from the detector when the detector is at $2\theta = 0$ or close to this value. Since the sample masks half of the direct beam, the beam center is no longer at $2\theta = 0$ but is offset at $2\theta = 0.5w$, where w is the HWHM of the direct beam in the absence of the sample. This effect can be clearly seen if the detector is made to scan with the sample fixed at $\alpha = 0$ (see Fig. 4). The intensity measured during such a scan and normalized to the direct-beam intensity is given by

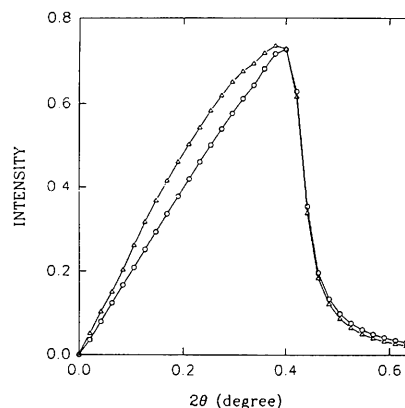$$I(2\theta) = G(2\theta - 0.5w) * \Pi_w(2\theta),$$
(13)

Fig. 3. Calculated reflectivity with a linear (open circles) and nonlinear (open triangles) correction for geometrical factors.

where $G(2\theta - 0.5w)$ denotes a Gaussian function with a center at $0.5w$ and a HWHM equal to w, and $\Pi_w(2\theta)$ is a step function of HWHM $= w$ characterizing the detector response.

This effect, which is clear in the 2θ scan of the detector (see Fig. 4) is also clearly visible during a θ-2θ scan when the sample length is not too large because, in this case, the edge of the sample cannot mask the direct beam during its rotation. The reflected intensity is then the sum of the direct beam and the intensity corrected from the geometrical factor according to (11).

The above correction applies only at low angle or low Q_z wavevector transfer and one may be tempted to avoid it by starting the measurement at some value of Q_z where the correction does not apply. This is certainly a possible choice but then it becomes difficult to determine the absorption of the X-ray beam into the sample. Indeed, the effect of the absorption is clearly visible below the critical angle, where the geometrical correction applies. As first noted by Parrat (1954), it is absorption that makes the reflectivity deviate from unity below the critical angle. Above this limit of total reflection, absorption still plays an important role but competes with the usual decrease of the reflectivity according to Fresnel's law and with the contribution from the interfacial roughness, so that it becomes more difficult to determine the contribution of each factor. This statement is enhanced by the fact that even a 'pure' sample is frequently composed of multiple slabs that do not have the same critical angle and absorption. Let us recall that the experimental quantity obtained in a reflectivity measurement is the square of the modulus of the reflection coefficient, $|r|^2$, which can be calculated from the electron density depth profile in the

material. However, it is well known that ambiguities can arise in the calculation because the solution is generally nonunique given the high nonlinearity of the expression for $|r|^2$. For this reason, a measurement of the specular reflectivity below the critical angle presents the clear advantage that determination of the absorption is possible provided the geometrical corrections are made.

A final correction has to be applied to the calculated reflected intensity and is due to resolution-function effects.

III.2. The resolution-function correction

In addition to the above geometrical correction, one has to correct the calculated reflectivity for resolution effects because the resolution function is not an exact δ function.

The wavevector transfer Q (see Fig. 5) is given by

$$\mathbf{Q} = \mathbf{k}_d - \mathbf{k}_0. \qquad (14)$$

For an elastic process, the outgoing wavevector has the same magnitude as the incoming wavevector and Q has in the (x, z) system of axes two components,

$$Q_x = k_0(\cos \alpha - \cos \beta), \qquad (15a)$$

$$Q_z = k_0(\sin \alpha + \sin \beta), \qquad (15b)$$

where α and β are the angles made by the incoming and outgoing waves with respect to the surface of the sample and $k_0 = 2\pi/\lambda$. We do not take into account the Q_y dependence (which is the out-of-plane component) because in this direction the size of the slits is large enough to integrate the scattered intensity. The differentials of these equations with respect to the variables α, β and k_0 are

$$dQ_x = -k_0(\sin \alpha \, d\alpha - \sin \beta \, d\beta)$$
$$+ dk_0(\cos \alpha - \cos \beta), \qquad (16a)$$

$$dQ_z = k_0(\cos \alpha \, d\alpha + \cos \beta \, d\beta)$$
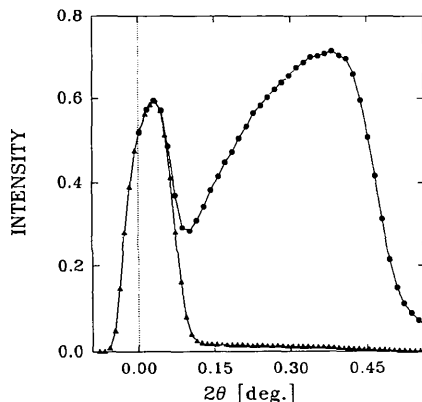$$+ dk_0(\sin \alpha + \sin \beta), \qquad (16b)$$

Fig. 4. Measured reflectivity curve of a silicon wafer of width 34 mm showing the presence of the direct beam at a location different from $2\theta = 0$. Filled triangles describe the scan of the detector when the sample is kept at the fixed position $\alpha = 0$ and full circles the result of a θ-2θ scan. The continuous lines joining the points are merely visual guides.
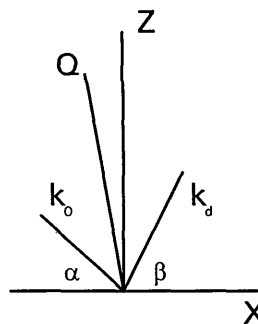

Fig. 5. Schematical representation of the wavevector transfer Q in the X, Z system of coordinates.

where dk_0 is related to the wavelength dispersion by

$$dk_0 = -k_0 \, d\lambda/\lambda. \tag{17}$$

With the assumption that $d\alpha$ and $d\beta$ are randomly distributed, the uncertainties in Q_x and Q_z are given by

$$\Delta Q_x^2 = k_0^2(\sin^2 \alpha \, \Delta\alpha^2 + \sin^2 \beta \, \Delta\beta^2)$$
$$+ \Delta k_0^2(\cos \alpha - \cos \beta)^2, \tag{18a}$$

$$\Delta Q_z^2 = k_0^2(\cos^2 \alpha \, \Delta\alpha^2 + \cos^2 \beta \, \Delta\beta^2)$$
$$+ \Delta k_0^2(\sin \alpha + \sin \beta)^2. \tag{18b}$$

For specular reflectivity, the incoming and outgoing angles α and β are equal to the Bragg angle θ so that the resolution-function HWHM along x and z are

$$\Delta Q_x = k_0 \sin \theta (\Delta\alpha^2 + \Delta\beta^2)^{1/2}, \tag{19a}$$

$$\Delta Q_z = [k_0^2 \cos^2 \theta (\Delta\alpha^2 + \Delta\beta^2) + 4\Delta k_0^2 \sin^2 \theta]^{1/2}. \tag{19b}$$

For specular reflectivity measurements, θ is always very small and $\Delta k_0 \sin \theta$ is negligible in (19b), so

$$\Delta Q_z = k_0 \cos \theta (\Delta\alpha^2 + \Delta\beta^2)^{1/2}. \tag{20}$$

With the introduction of the HWHM of the direct-through beam given by w,

$$w = 2\Delta\theta = (\lambda/2\pi) \, \Delta Q_z|_{2\theta=0}$$
$$= (\Delta\alpha^2 + \Delta\beta^2)^{1/2}, \tag{21}$$

it follows that

$$\Delta Q_x = Q_z w/2, \tag{22a}$$

$$\Delta Q_z = k_0 w \cos \theta. \tag{22b}$$

Equations (22a, b) are very important because they give the theoretical values of the HWHM of the resolution function in the x, z system of axes. Equation 22(a) shows that the width of the resolution

Table 1. *Typical parameters used in the calculation of the reflectivity of the silicon wafer*

The parameter σ denotes the roughness of the interface, τ is the layer thickness, μ is the imaginary part of the index of refraction and q_c the critical value for total external reflection of the wavevector transfer.

	q_c (Å^{-1})	μ	σ (Å)	τ (Å)
Si	0.032	1.1×10^{-7}	1	—
Top layer	0.0265	9.7×10^{-8}	3	17.2

function in the Q_x direction is proportional to Q_z. This means that the angular width $\Delta\Psi$ of the resolution function is constant whatever the Q_z position along the ridge and is equal to

$$\Delta\Psi = w/2. \tag{23}$$

If this condition is not fulfilled, this is a sign that the sample is bent on a macroscopic scale and the absolute reflectivity is consequently reduced by a factor equal to $2\Delta\Psi/w$ at least when the footprint of the beam is larger than the sample size.

Equation (22b) shows that at small angles of incidence the width of the resolution function in the longitudinal direction for the Q_z scan is almost constant and is equal to k_0w.

As a result, the absolute measured reflectivity should be compared with the convolution of the corrected calculated intensity with the resolution function, which will be assumed to be Gaussian with a HWHM of k_0w. The final expression for the reflected intensity in this case is given by

$$I(Q_z) = [I_c(Q_z) + \delta(Q_z - k_0w/2)]g_{k_0w}(Q_z), \tag{24}$$

where $I_c(Q_z)$ is the corrected calculated intensity according to (11), $\delta(Q_z - k_0w/2)$ is a delta function that describes the direct-beam contribution and $g(Q_z)$ is the Gaussian resolution function.
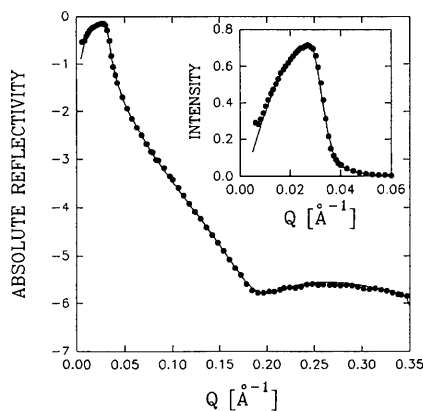

Fig. 6. Calculated (solid line) and observed reflectivities (filled circles) of a silicon wafer. The insert shows on a linear scale the calculated and observed reflectivities for small magnitudes Q.
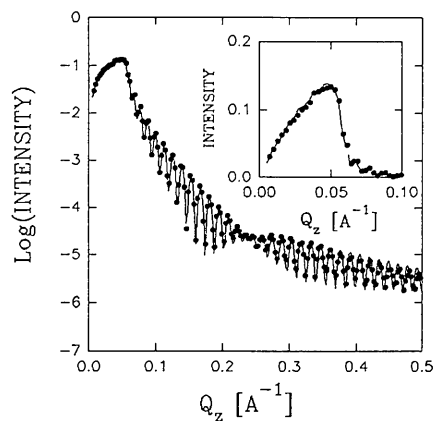

Fig. 7. Calculated (solid line) and observed reflectivities (filled circles) of a niobium film on sapphire. The insert shows on a linear scale the part of the reflectivity curve for small Q_z.

To perform the convolution correctly, it is necessary to calculate the reflected intensity in the same way as for the Gaussian function. Fig. 6 describes the results of the calculated reflectivity of a silicon wafer of width 35 mm in the case of a Q_z scan along the ridge. The insert shows on a linear scale how the geometrical correction gives a good estimation at small Q_z of the measured intensity. The computation was performed with the matrix technique (Born & Wolf, 1964) with help of Matlab software (Gibaud & Vignaud, 1993). The electron density depth profile for this silicon wafer can be separated from the calculation, showing the presence of a layer of thickness 17.2 Å at the surface of the bulk silicon. Typical parameters used in the calculation are reported in Table 1. The low electron density of the surface layer reveals that it is probably related more to water deposition than to an oxide deposition. In conclusion, the above corrections strongly depend upon the line shape of the direct beam. When slits and a graphite analyzer (low-resolution mode) are used, the line shape is Gaussian but, in the case of a high-resolution triple-crystal diffractometer (Ge monochromator-crystal–Ge analyzer), the beam line shape is Lorentzian, so a Lorentzian function must be used to perform the corrections. This is illustrated in Fig. 7, which represents the absolute reflectivity of a niobium film on top of a sapphire substrate. The insert shows the observed and corrected calculated reflectivities.

In this case, the contamination by the direct beam is not a problem because the FWHM of the direct beam in this high-resolution mode is only 0.01° (cf. 0.1° for the low-resolution mode). The geometrical correction is in this case very severe because the sample was only 10 mm wide and the beam 200 µm thick; this is clearly illustrated by the fact that the reflectivity was far less than 1 at $Q = Q_c$.

References

ALS-NIELSEN, J. (1984). Physica (Utrecht), B126, 145–155.
BENATAR, J. J. (1992). Recherche, 244, 723–728.
BORN, M. & WOLF, E. (1964). Principles of Optics. Oxford: Pergamon Press.
BRUGEMANN, L., BLOCH, R., PRESS, W. & GERLACH, P. (1990). J. Phys. Condens. Matter, 2, 8869–8878.
GIBAUD, A. & VIGNAUD, G. (1993). In preparation.
PARRAT, L. G. (1954). Phys. Rev. 95, 359–369.
RUSSEL, T. (1990). Mater. Sci. Rep. 5, 171–272.
SINHA, S. K. (1991). Physica (Utrecht), B173, 25–34.

The Arrangement of Point Charges with Tetrahedral and Octahedral Symmetry on the Surface of a Sphere with Minimum Coulombic Potential Energy

BY J. R. EDMUNDSON

Photosol Ltd, 15 Bakers Court, Paycocke Road, Basildon, Essex SS14 3EH, England

(Received 14 September 1992; accepted 27 January 1993)

Abstract

Up to 100 point charges have been distributed on the surface of a sphere such that the configurations display T and O symmetry as well as being a minimum, global or local, with respect to the Coulombic potential.

Introduction

The symmetry adopted by N point charges on the surface of a sphere such that the Coulombic potential is a minimum has been determined by several investigators: Ashby & Brittin (1986); Edmundson (1992); Erber & Hockney (1991); Frickel & Bronk (1987); Melnyk, Knop & Smith (1977); Rafac, Schiffer, Hangst, Dubin & Wales (1991); Weinrach, Carter, Bennett & McDowell (1990); Wille (1986).

Table 1 lists the values of N when the arrangements display tetrahedral or octahedral symmetry. This paper describes which other values of N can display T and O symmetries and at the same time produce a local minimum in terms of the Coulombic potential.

Tetrahedral configurations

The tetrahedron differs from the other Platonic solids in that it is its own dual and has no centre of